Sensors & Transducers, Vol. 177, Issue 8, August 2014, pp. 177-183

Sensors & Transducers

Analysis of Energy Transmission Modes of Flyback Converter

[1] GONG Shu, [2] GONG Ren-Xi, [3] WANG Kuang
College of Electrical Engineering, Guangxi University, Nanning 530004, Guangxi, China
Tel.: +86-0771-3291765
E-mail: 871009450@qq.com, rxgong@gxu.edu.cn, 1678005365@qq.com

Received: 21 March 2014 /Accepted: 31 July 2014 /Published: 31 August 2014

Abstract: It is of significance to investigate energy transmission modes of a flyback converter for its optimum design. In this paper, the ETMs of a flyback converter are divided into three modes, which are continuous conduction mode-complete inductor supply mode, continuous conduction mode-incomplete inductor supply mode and discontinuous conduction mode-incomplete inductor supply mode, respectively. A deep analysis of the operation is made, a reduction of the boundary condition between the modes is conducted and a comparison of current stress, transformer AP and output ripple voltage between the modes is performed. A 30W prototype is developed and its experiment is done. The experiment results are in agreement with the theoretical analysis quite well. *Copyright © 2014 IFSA Publishing, S. L.*

Keywords: Energy transmission modes, Flyback converter, Continuous conduction mode-complete inductor supply mode, Continuous conduction mode-incomplete inductor supply mode, Discontinuous conduction mode-incomplete inductor supply mode.

1. Introduction

A flyback converter has been widely used in the low-power rate power supplies because of its simple structure, low cost and easy implementation of multiple outputs etc. [1-4]. By comparing the current through the rectifying diode with output current, the energy transmission modes (ETMs) of DC/DC converter can be divided into:

1) Continuous conduction mode (CCM) and discontinuous conduction mode (DCM),

2) Complete inductor supply mode (CISM) and incomplete inductor supply mode (IISM).

The former is practical for investigating the power circuit [5-8], while the latter is useful for analyzing the output ripple voltage [9, 10]. As a matter of the fact, the energy transmission process of a flyback converter can not be completely described by any of them. In order to represent the converter comprehensively, the energy transmission modes (ETMs) of a flyback converter are proposed to be divided into CCM-CISM, CCM-IISM and DCM-IISM in this paper. An analysis of the operation and boundary conditions is made and a comparison of current stress, transformer AP and output ripple voltage between the modes is performed.

2. Definitions of the Three Energy Transmission Modes

The topology of a flyback converter is shown in Fig. 1, of which L_p, L_s, n, S, D_o, C_o, R_o are primary inductor, secondary inductor, turn ratio which is defined as $L_p=n^2L_s$, the main switch, the rectifying diode, smoothing capacitor and load resistance

respectively. During the period when the switch S is on, and the diode D_o is off, the energy will be stored in the transformer. The ripple current and peak current of primary current $i_p(t)$ can be expressed as

$$\Delta I = \frac{V_g D}{L_p f_s}, \tag{1}$$

and

$$I_{p,\max} = \frac{V_o I_o}{D V_g} + \frac{\Delta I}{2}, \tag{2}$$

where f_s, V_o and I_o are the switching frequency, the average value of output voltage and the average value of output current respectively, and D is the ratio of conduction time of the switch S to switching period.

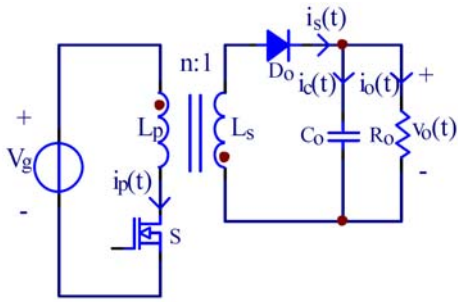

Fig. 1. Topology of flyback converter.

During the period when the switch S is off, while the diode D_o is on, the energy is released by the transformer. The minimum current through D_o is given as

$$I_{s,\min} = nI_{p,\max} - \frac{V_o D'}{L_s f_s}, \tag{3}$$

where D' is defined as the ratio of conduction time of D_o to switching period. In CCM, $D + D' = 1$.

According to the relationship of the voltage-second balance, the following expression can be obtained:

$$V_g D = nV_o D', \tag{4}$$

If the $I_{s,min}$ equals I_o at the end of a switching period, the boundary primary inductor between CCM-CISM and CCM-IISM is obtained by substituting Eqs.(2)-(4) into Eq. (1),

$$L_k = \frac{nD'V_g}{2 f_s I_o}, \tag{5}$$

If the $I_{s,min}$ equals zero at the end of a switching period, the boundary primary inductor between CCM-IISM and DCM-IISM is derived by substituting Eqs.(2), (3) and (4) into Eq.(1),

$$L_c = \frac{nD' DV_g}{2 f_s I_o} = DL_k, \tag{6}$$

As result of $D < 1$, the following relationship can be obtained:

$$L_c < L_k, \tag{1}$$

Eqs. (5) to (7) indicate that the ETMs of a flyback converter depend on the primary inductor L_p and can be precisely defined as follows:

1) A flyback converter operates in CCM-CISM if $L_k < L_p$.

2) A flyback converter operates in CCM-IISM if $L_c < L_p < L_k$.

3) A flyback converter operates in DCM-IISM if $L_p < L_c$.

The key waveforms of three ETMs are shown in Fig. 2.

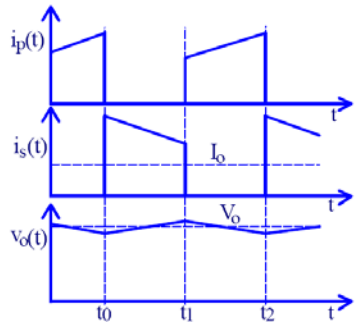

(a) CCM-CISM

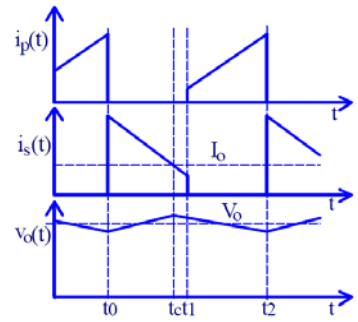

(b) CCM-IISM

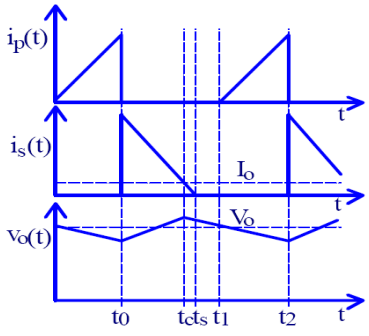

(c) DCM-IISM

Fig. 2. Key waveforms of flyback converter.

Fig. 2 shows that only C_o supplies R_o with power during the interval [t_1-t_2] of the on-state of *S*, while the energy of R_o is supplied by L_p or C_o during the interval [t_0-t_1] of the off-state of *S*. The energy transmission processes during the off-state of *S* are described in detail:

1) CCM-CISM: a flyback transformer continuously supplies R_o with power and charges *C* up during the interval [t_0-t_1].

2) CCM-IISM: a flyback transformer supplies R_o and C_o with energy during the interval [t_0-t_c], then both transformer and C_o supply R_o with energy during the interval [t_c-t_1].

3) DCM-IISM: the energy transmission process is same as that of CCM-IISM during the interval [t_0-t_s]. However, the energy of R_o is solely supplied by C_o during the interval [t_s-t_1], which is because the transformer has released all the stored energy.

3. Analysis and Comparison of the Three Energy Transmission Modes

3.1. Branch Currents

Now, geometric analysis approach is used to make the comparison of the branch currents. Primary current of a flyback transformer is shown in Fig. 3, where V_g/L_p is the slope of $i_p(t)$, the trapezoid ABCD represents the boundary waveform between CCM-CISM and CCM-IISM and the triangle ABE represents the boundary waveform between CCM-IISM and DCM-IISM.

According to energy conservation theory, the waveform areas should be equal to the variation of L_p.

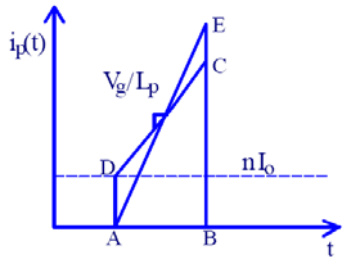

Fig. 3. Primary current waveform of flyback transformer.

The relationships of the peak current and the ripple current of $i_p(t)$ between the three ETMs are clearly shown in the Fig. 3.

$$\Delta I_{CC} < \Delta I_{CI} < \Delta I_{DI}, \tag{8}$$

$$I_{p,\max\_CC} < I_{p,\max\_CI} < I_{p,\max\_DI}, \tag{9}$$

where *CC*, *CI* and *DI* in subscript are the abbreviation of CCM-CISM, CCM-IISM and DCM-IISM respectively.

The RMS value of $i_p(t)$ can be expressed as

$$I_{p,rms} = \sqrt{\frac{1}{T}\int_0^{DT} i_p^{\,2}(t)dt} = I_{p,\max}\sqrt{D(\frac{K_{rp}^{\,2}}{3} - K_{rp} + 1)}, \tag{10}$$

where $0 \le K_{rp} \le 1$ and K_{rp} is defined as

$$K_{rp} = \frac{\Delta I}{I_{p,\max}}, \tag{11}$$

The RMS current of the triangle waveform ABE divided by the RMS current of trapezoid waveform ABCD yields:

$$\alpha = \frac{2 - K_{rp}}{\sqrt{K_{rp}^{\,2} - 3K_{rp} + 3)}} \ge 1, \tag{12}$$

where α is the monotonously decreasing function of K_{rp} at the range [0, 1].

In terms of Eqs. (8) and (9), the relationship of K_{rp} among the three modes can be expressed as

$$K_{rp\_CC} < K_{rp\_CI} < K_{rp\_DI}, \tag{13}$$

Consequently, the relationship of $I_{p,rms}$ among three modes can be derived as:

$$I_{p,rms\_CC} < I_{p,rms\_CI} < I_{p,rms\_DI}, \tag{14}$$

The RMS value of $i_s(t)$ can be expressed as

$$I_{s,rms} = \sqrt{\frac{1}{T}\int_{DT}^{T} i_s^{\,2}(t)dt} = nI_{p,\max}\sqrt{D'(\frac{K_{rp}^{\,2}}{3} - K_{rp} + 1)}, \tag{15}$$

Similarly, the following relationships can be achieved by comparing the peak and RMS current of $i_s(t)$:

$$I_{s,\max\_CC} < I_{s,\max\_CI} < I_{s,\max\_DI}, \tag{16}$$

$$I_{s,rms\_CC} < I_{s,rms\_CI} < I_{s,rms\_DI}, \tag{17}$$

The RMS value of $i_c(t)$ can be expressed as

$$I_{c,rms} = \sqrt{I_{s,rms}^{\,2} - I_o^{\,2}}, \tag{18}$$

From Eqs.(17) and (18), we get

$$I_{c,rms\_CC} < I_{c,rms\_CI} < I_{c,rms\_DI}, \tag{19}$$

3.2. AP Value of Transformer

The effective cross-sectional area A_e can be formulated by

$$A_e = \frac{V_g D}{N_p \Delta B f_s}, \tag{20}$$

where N_p is the primary turns and ΔB is the magnetic flux density swing which is defined as

$$\Delta B = \frac{0.4\pi N_p \Delta I}{l_g + l_m / \mu_r}, \quad (21)$$

where l_g, l_m and u_r are the airgap length, effective magnetic path length and relative permeability respectively.

Similarly, the maximum of magnetic flux density swing can be written by

$$B_{\max} = \frac{0.4\pi N_p I_{p,\max}}{l_g + l_m / \mu_r}, \quad (22)$$

From Eqs.(18) and (19), we have

$$\frac{\Delta B}{B_{\max}} = \frac{\Delta I}{I_{p,\max}} = K_{rp}, \quad (23)$$

In addition, the core window area is

$$A_w = \frac{N_p I_{p,rms}}{J K_p K_u}, \quad (24)$$

where J, K_p and K_u are the copper current density, primary turns area coefficient and the window effective area coefficient respectively.

From Eqs.(21), (23) and (24), the AP value of the transformer can be derived as:

$$AP = A_e A_w = \frac{V_g D I_{p,rms}}{J K_p K_u K_{rp} B_{\max} f_s}, \quad (25)$$

The ratio of the AP value corresponding to the triangle waveform ABE to that of the trapezoid waveform ABCD, yields

$$\beta = \frac{(2 - K_{rp}) K_{rp}}{\sqrt{K_{rp}^2 - 3K_{rp} + 3)}} \le 1, \quad (26)$$

where β is the monotonously incremental function of K_{rp} at the interval [0, 1].

From Eqs. (25) and (26), the relationship of the value AP of the transformer among three modes can be written as:

$$AP_{CC} > AP_{CI} > AP_{DI}, \quad (27)$$

3.3. Output Ripple Voltage

As shown in Fig. 2(a), the increment of $V_o(t)$ at the interval $[t_0,t_1]$ should be equal to the decrement of $V_o(t)$ at $[t_1,t_2]$. The output ripple voltage in CCM-CISM can be derived as

$$\Delta V_{C,CC} = -\frac{1}{C_o}\int_0^{DT} -I_o dt = \frac{I_o DT}{C_o}, \quad (28)$$

Solving D from Eq.(4),one obtains:

$$D = \frac{nV_o}{V_g + nV_o}, \quad (29)$$

Substitution of Eq.(29) into Eq.(28), yields

$$\Delta V_{C,CC} = \frac{nV_o I_o}{f_s C_o (V_g + nV_o)}, \quad (30)$$

Eq.(30) shows that $\Delta V_{C,CC}$ is independent on L_p.

As shown in Fig. 2(b) and Fig. 2(c), C_o is charged by transformer through D_o during the interval $[t_0\text{-}t_c]$. The charging time Δt and charging current i_c(t) can be expressed as

$$\Delta t = t_c - t_0 = (nI_{p,\max} - I_o)\frac{L_s}{V_o}, \quad (31)$$

$$i_c(t) = nI_{p,\max} - \frac{V_o}{L_s}t - I_o, \quad (32)$$

The output ripple voltage in CCM-IISM and DCM-IISM can be derived as

$$\Delta V_C = \frac{1}{C_o}\int_0^{\Delta t} i_c(t)dt = \frac{L_s}{2C_o V_o}(nI_{p,\max} - I_o)^2, \quad (33)$$

In CCM-IISM, $I_{p,max}$ can be solved from Eqs.(1) and (2)

$$I_{p,\max} = \frac{V_g D}{2L_p f_s} + \frac{V_o I_o}{D V_g}, \quad (34)$$

By substituting Eq.(34) and $L_p = n^2 L_s$ into Eq.(33), the output ripple voltage in CCM-IISM can be expressed as

$$\Delta V_{C,CI} = \frac{1}{2V_o C_o L_p}\left[\frac{V_g D}{2 f_s} + (\frac{V_o I_o}{V_g D} - \frac{I_o}{n})L_p\right]^2, \quad (35)$$

The first order and second order of partial derivative of ΔV_{CI} with respect to L_p are respectively made, then the following expressions can be obtained:

$$\frac{\partial \Delta V_{CI}}{\partial L_p} = \frac{1}{2V_o C_o L_p^2}\left[(\frac{V_o I_o}{V_g D} - \frac{I_o}{n})^2 L_p^2 - (\frac{V_g D}{2 f_s})^2\right], \quad (36)$$

$$\frac{\partial^2 \Delta V_{CI}}{\partial^2 L_p} = \frac{V_g^2 D^2}{4 f_s^2 V_o C_o L_p^3} > 0, \quad (37)$$

By letting the right side of Eq.(36) be zero, an only stagnation point can be obtained:

$$L_p = \frac{nV_g{}^2 D^2}{2f_s(nV_oI_o - I_oDV_g)} = \frac{nD'V_g}{2f_sI_o} = L_k, \quad (38)$$

where ΔV_{CI} is the monotonously digressive function of L_p at the interval [L_c, L_k] since the second order of partial derivative is greater than zero.

In DCM-IISM, $I_{p,max}$ equals Δi. By substituting Eq.(1) and $L_p = n^2 L_s$ into Eq.(33), the output ripple voltage in DCM-IISM can be expressed as

$$\Delta V_{C,DI} = \frac{(nV_gD - L_pf_sI_o)^2}{2V_oC_oL_pn^2f_s{}^2}, \quad (39)$$

Eq. (39) shows that $\Delta V_{C,CC}$ is inversely proportional to L_p.

Up to now, the output ripple voltages have been derived under the assumption that the smoothing capacitor C_o is ideal. In practice, the equivalent series resistor (ESR) R_{esr} of the smoothing capacitor can not be neglected in the ripple voltage analysis. In any ETM, the ripple voltage across R_{esr} can be expressed as

$$\Delta V_R = nI_{p,\max}R_{esr}, \quad (40)$$

The total output ripple voltage is

$$\Delta V = \Delta V_C + \Delta V_R, \quad (41)$$

Substituting Eqs.(1), (30), (33), (35), (39) and (40) into (41), we obtain the output ripple voltage of three ETMs with ESR of the smoothing capacitor considered

$$\Delta V_{CC} = \frac{nI_oV_o}{C_of_s(V_g + nV_o)} + nR_{esr}\left(\frac{V_gD}{2L_pf_s} + \frac{V_oI_o}{DV_g}\right), \quad (42)$$

$$\Delta V_{CI} = \frac{1}{2V_oC_oL_p}\left[\frac{V_gD}{2f_s} + \left(\frac{V_oI_o}{V_gD} - \frac{I_o}{n}\right)L_p\right]^2 + nR_{esr}\left(\frac{V_gD}{2L_pf_s} + \frac{V_oI_o}{DV_g}\right), \quad (43)$$

$$\Delta V_{DI} = \frac{(nV_gD - L_pf_sI_o)^2}{2V_oC_oL_pn^2f_s{}^2} + \frac{nR_{esr}V_gD}{L_pf_s}, \quad (44)$$

4. Experiment Results

A prototype is made to verify the theoretical analysis. The key parameters of the converter are as follows:

V_g =100 V, V_o=12 V, I_o=2.5 A, R_o=4.8 Ω, f_s=66 kHz, n=8.5, J=4 A/mm^2, K_p=0.4, K_u=0.3, B_{max}=0.3 T, C_o=2000 μF, R_{esr}=20 mΩ.

Substituting the relative parameters into Eqs.(5) and (6), we get: L_k= 1.28 mH and L_c = 0.64 mH. As we know, all the branch currents, the AP value of the transformer and output ripple voltage vary with L_p. The comparison among three ETMs is made in the Table 1.

Table 1. Comparison between the three ETMs.

L_p (mH)	ΔI (A)	$I_{p,max}$ (A)	$I_{p,rms}$ (A)	$I_{s,max}$ (A)	$I_{s,rms}$ (A)
1.7	0.45	0.82	0.43	6.96	3.64
1.28	0.6	0.89	0.44	7.6	3.7
0.9	0.85	1.02	0.46	8.65	3.84
0.64	1.19	1.19	0.49	10.1	4.1
0.5	1.35	1.35	0.52	11.46	4.93
L_p (mH)	**$I_{c,rms}$ (A)**	**AP (mm^2)**	**ΔV_C (mV)**	**ΔV_R (mV)**	**ΔV (mV)**
1.7	2.64	4179	9.56	139.25	148.81
1.28	2.73	3490	9.56	151.8	161.36
0.9	2.92	2915	9.85	172.95	182.8
0.64	3.25	2590	10.72	202	212.72
0.5	4.25	2431	11.58	229.21	240.79

The key experimental waveforms are shown in Fig. 4. The experimental results are approximately in agreement with the theoretical calculations. But two differences should be pointed out:

1) As shown in Fig. 4(a) and Fig. 4(c), the measured ripple and peak current of i_p(t) are a little greater than the calculated values since the conversion efficiency is less than 1 due to the existence of the parasitic components [11-14].

2) From Fig. 4(b) and Fig. 4(d), it can be seen that the AC components of v_o(t) are composed of ripple and noise. The switching noise is caused by the parasitic components and it is often desirable to add a post LC filter to suppress it.

5. Conclusions

An investigation of the energy transmission modes of a flyback converter is made and a comparison of the three modes proposed is performed. A 30 W prototype is developed and tested. The experimental results agree with the theoretical analysis. Accordingly, the following conclusions can be drawn:

1) The current stress is smallest and the AP value of transformer is biggest in CCM-CISM, both current stress and the AP value of transformer is medium in CCM-IISM and current stress is biggest and the AP value of transformer is smallest in DCM-IISM.

2) If the ESR of the smoothing capacitor is neglected, the ripple voltage in CCM-CISM is smallest and is independent on L_p, that in CCM-IISM is medium and is inversely proportional to L_p, and that in DCM-IISM is biggest and vary inversely with L_p. This conclusion is similar to the reference [9] in which the ETMs of boost converters are analyzed. If the ESR of the smoothing capacitor is considered, the ripple voltage decreases with increased L_p in any ETM.

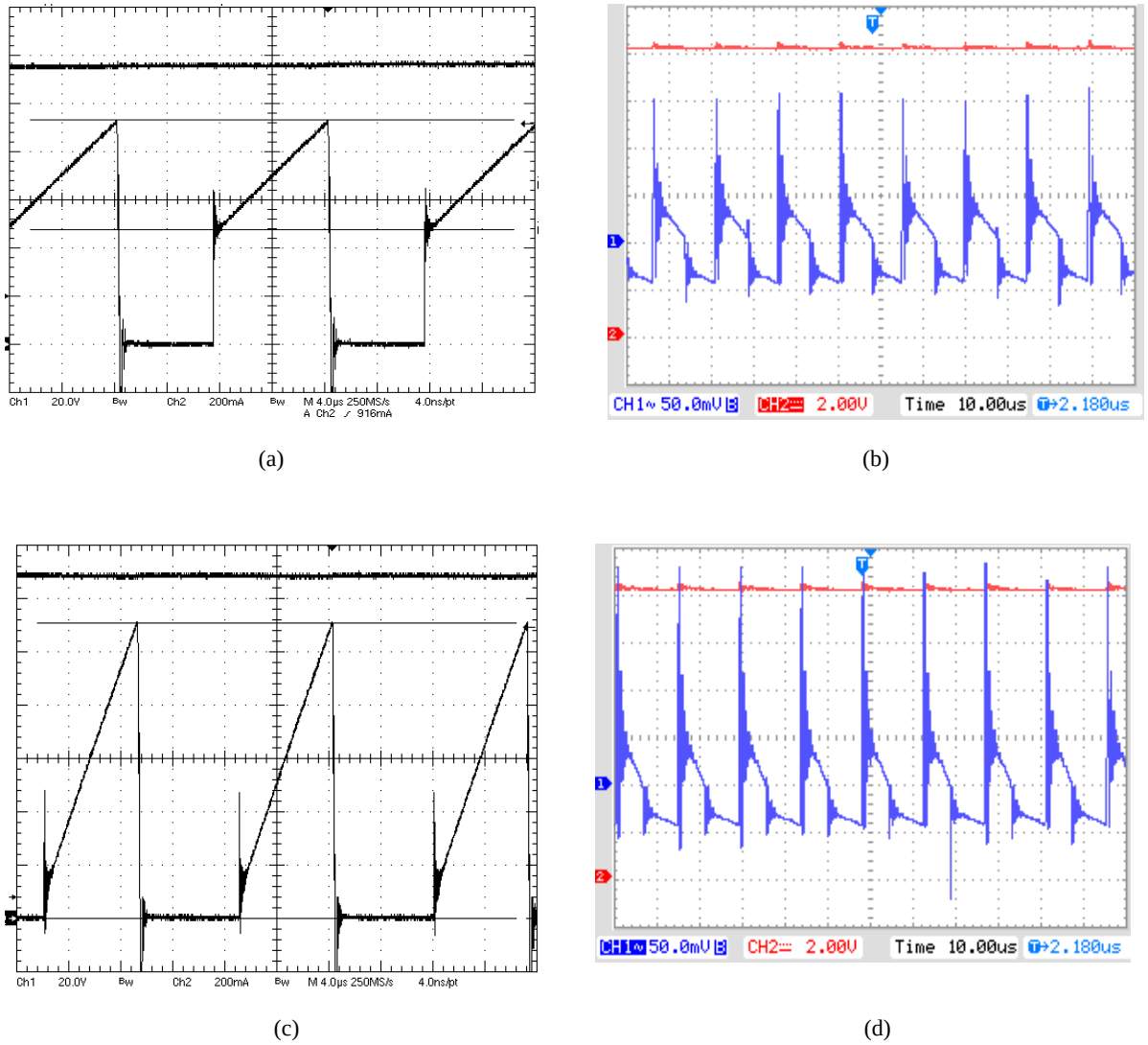

Fig. 4. Key experimental waveforms: (a) CH1=V_g CH2=$i_p(t)$ when L_p=1.7 mH, (b) CH1=△V CH2=V_o when L_p =1.7 mH, (c) CH1= V_g CH2= $i_p(t)$ when L_p =0.9 mH, (d) CH1=△V CH2= V_o when L_p =0.9 mH.

Acknowledgements

The research was supported by Guangxi Natural Science Foundation of China (Grant No. 2010GXNSFA013023) and Nanning Scientific Research & Development Foundation of Guangxi, China (Grant No. 20121025).

References

[1]. Hsing-Fu Liu, Lon-Kou Chang, Flexible and low cost design for a flyback AC/DC converter with harmonic current correction, *IEEE Transactions on Power Electronics*, Vol. 20, Issue 1, 2005, pp. 17-24.

[2]. Jong-Jae Lee, Jung-Min Kwon, Eung-Ho Kim, et al, Single-stage single-switch PFC flyback converter using a synchronous rectifier, *IEEE Transaction on Industrial Electronics*, Vol. 55, Issue 3, 2008, pp. 1352-1365.

[3]. H. M. Pang, P. M. H. Bryan, A stability issue with current mode control flyback converter driving LEDs, in *Proceedings of IEEE 6th International Power Electronics and Motion Control Conference*, Wuhan, China, 17-20 May 2009, pp. 1402-1406.

[4]. Ki-Bum Park, Chong-Eun Kim, Gun-Woo Moon, et al, PWM resonant single-switch isolated converter, *IEEE Transactions on Power Electronics*, Vol. 24, Issue 8, 2009, pp. 1876-1886.

[5]. J. Sun, D. M. Mitchell, M. F. Greuel, P. T. Krein, et al, Averaged modeling of PWM converters operating in discontinuous conduction mode, *IEEE Transactions on Power Electronics*, Vol. 16, Issue 4, 2001, pp. 482-492.

[6]. Nikolaos P. Papanikolaou, Emmanuel C. Tatakis, Active voltage clamp in flyback converters operating in CCM mode under wide load variation, *IEEE Transaction on Industrial Electronics*, Vol. 51, Issue 3, 2004, pp. 632-640.

[7]. Tzuen-Lih Chern, Li-Hsiang Liu, Ping-Lung Pan, et al, Single-stage flyback converter for constant current output LED driver with power factor correction, in *Proceedings of International Conference on Industrial Electronics and Applications*, Xi'an, China, 25-27 May 2009, pp. 2891-2896.

[8]. Yuan-Chil Chang, Chang-Ming Liaw, Design and control for a charge-regulated flyback switch-mode rectifier, *IEEE Transactions on Power Electronics*, Vol. 24, Issue 1, 2009, pp. 59-74.
[9]. Liu Shulin, Liu Jian, Yang Yinling, et al, Energy transmission modes and output ripple voltage of Boost converters, *Proceedings of the CSEE*, Vol. 26, Issue 5, 2006, pp. 119-124.
[10]. Liu Shulin, Liu Jian, Kou Lei, et al, Analysis of output ripple voltage of Buck DC/DC converters and its application, *Transactions of China Electrotechnical Society*, Vol. 22, Issue 2, 2007, pp. 91-97.
[11]. C. Larouci, J.-P. Keradec, J.-P. Ferrieux, et al, Copper losses of flyback transformer: search for analytical expressions, *IEEE Transactions on Magnetics*, Vol. 39, Issue 3, 2003, pp. 1745-1748.
[12]. A. Hren, J. Korelic, M. Milanovic, RC-RCD clamp circuit for ringing losses reduction in a flyback converter, *IEEE Transactions on Circuits and Systems*, Vol. 53, Issue 5, 2006, pp. 369-373.
[13]. Haiyan Lu, Jianguo Zhu, S. Y. R. Hui, Experimental determination of stray capacitances in high frequency transformers, *IEEE Transactions on Power Electronics*, Vol. 18, Issue 5, 2003, pp. 1105-1112.
[14]. Himanshu K. Patel, Voltage transient spikes suppression in flyback converter using dissipative voltage snubber, in *Proceedings of the International Conference on Industrial Electronics and Applications*, Singapore, 3-5 June 2008, pp. 897-901.